Research Article

Automated Image Quality Classification In 99mtc-MDP Bone Scintigraphy: An Unsupervised Approach Using PCA And K- Means Clustering

Arun K. Bashambu[1], Dr. Manisha Agarwal[2], Dr. Shallu Bashambu[3], Arushi Bashambu[4]

[1]Scholar CSE Dept, Banasthali Vidyapith, Banasthali Jaipur, India. Email: arunbashambu@rediffmail.com.
[2*]Professor CSE Dept, Banasthali Vidyapith, Banasthali Jaipur, India. Email: manishaagarwal18@yahoo.co.in.
[3]Associate Professor IT Dept, MAIT New Delhi, India. Email: shallubashambu@mait.ac.in.
[4]Senior Software Engineer, Capgemini, Bangalore. Email: arushibashambu@gmail.com.

Abstract

Poor-quality images hinder clinical interpretation, while high-quality images are essential for both training and real-world deployment of AI/ML-based diagnostic tools. Reliable image quality assessment (IQA) is therefore crucial for the development of image enhancement algorithms, particularly in nuclear medicine, where diagnostic accuracy relies heavily on image clarity. Traditional subjective IQA methods are time-consuming, costly, and prone to inter-observer variability. Although various supervised learning-based approaches can be effective, they require large annotated datasets, which are often difficult to obtain in clinical practice. In this study, we propose a novel unsupervised IQA framework for 99mTc- MDP bone scintigraphy images using Principal Component Analysis (PCA) and K-means clustering. A dataset of 406 bone scans was processed using PCA for dimensionality reduction, retaining the top 32 principal components. K-means clustering (with k = 3) was then applied to classify images into three quality categories: 'Poor,' 'Good,' and 'Excellent.' The method was validated using 100 randomly selected images labeled by a nuclear medicine physician. The framework achieved an accuracy, sensitivity and specificity of 93%, 93.12% and 96.48% respectively, demonstrating its effectiveness. This unsupervised, interpretable, and data-efficient approach provides a practical solution for automated quality control in nuclear imaging workflows, with the potential to enhance both clinical decision-making and AI-based diagnostics.

Index Terms—Image quality assessment, unsupervised learning, nuclear medicine, 99mTc-MDP bone scintigraphy, PCA, clustering, k-means.

1. INTRODUCTION

Objective Image Quality Assessment (IQA) remains a fundamental yet challenging problem in medical imaging. While considerable research has been dedicated to IQA in natural images [1], relatively less attention has been directed toward planar nuclear medicine imaging, particularly technetium-99m methylene diphosphonate (99mTc-MDP) bone scintigraphy. These scans are critical for the detection of skeletal metastases, trauma, and metabolic bone diseases. However, their diagnostic value can be significantly affected by artifacts caused by patient movement, suboptimal radiopharmaceutical distribution, and hardware-related noise [2].

Supervised learning based approaches have shown promise in automated IQA systems [3],[4]. However, their adoption in nuclear medicine is hindered by the need for large-scale annotated datasets, as these resources are often costly, time-intensive, and challenging to obtain due to the need for experts. This motivates us to explore the potential of unsupervised machine learning approaches, which can identify meaningful patterns and structures in data without relying on labeled examples.

In this study, we propose a fully unsupervised IQA framework specifically designed for 99mTc-MDP bone scintigraphy. Our approach draws upon principles from perceptual quality modeling [5] and contemporary statistical learning methods. Principal Component Analysis (PCA) is employed for dimensionality reduction, capturing dominant modes of variation in image features. Subsequently, k-means clustering is utilized to categorize the images based on shared visual characteristics. We hypothesize that this combination of techniques can reveal hidden quality groups that match how humans judge diagnostic usefulness, thereby providing a scalable, interpretable, and annotation-free solution for quality control in nuclear medicine imaging workflows.

2. MATERIALS AND METHODS

A. Dataset

This study utilized a dataset comprising 203 whole- body bone scintigraphy studies performed using technetium-99m methylene diphosphonate (99mTc- MDP). Each study included paired anterior and posterior planar images, resulting in a total of 406 images. All scans were acquired under standard clinical imaging protocols. The DICOM images were anonymized in accordance with Institutional Review Board (IRB) protocols and ethical guidelines. To enable computational processing and uniform analysis, all images were resampled to a resolution of 128 × 128 pixels.

B. Preprocessing

Each image was reshaped into a one-dimensional feature vector. To mitigate the influence of acquisition variability, pixel intensities were normalized to a consistent dynamic range. This standardization ensured that subsequent feature extraction focused on structural features relevant to image quality rather than artifacts introduced during acquisition.

C. Dimensionality Reduction using Principal Component Analysis (PCA)

Principal Component Analysis (PCA) was applied to the normalized image vectors to reduce dimensionality while preserving the most informative visual features. Principal components were retained at three levels: 2, 3, and 32, capturing approximately 45%, 55%, and over 95% of the total variance in the dataset, respectively. These components were then used as input for K-means clustering, with the number of clusters set to $k = 3$. PCA has been widely adopted in biomedical imaging due to its ability to extract orthogonal directions of maximum variance, enabling effective feature reduction without substantial information loss [6].

D. Unsupervised Clustering with K-Means

To categorize image quality in an unsupervised manner, the k-means clustering algorithm was applied to the PCA-transformed data. A value of $k = 3$ was chosen based on clinical expectations of three distinct quality categories: poor, good, and excellent. The elbow method and visual cluster separation in the t-SNE space further supported this choice. To ensure clustering stability, the algorithm was initialized 10 times with random seeds, and the solution with the lowest within-cluster sum of squares was selected. K-means was chosen for its simplicity, computational efficiency, and established utility in radiological image grouping tasks [7].

E. Evaluation Metrics

Cluster performance was evaluated using both qualitative and quantitative approaches. A t-distributed Stochastic Neighbor Embedding (t-SNE) visualization was used to assess the separability of clusters in the reduced PCA space. Additionally, a subset of 100 images from 50 randomly selected studies was independently reviewed and labeled by a senior nuclear medicine physician with over 20 years of experience. Images were classified into three categories (poor, good, and excellent) based on established clinical criteria. These expert labels served as a reference standard for evaluating the clustering performance. Agreement between expert and algorithm-generated classifications was assessed using confusion matrices and overall classification accuracy.

F. DICOM Metadata Extraction and Analysis

To complement the image-based analysis, acquisition- related metadata were extracted from the DICOM headers of all 203 bone scintigraphy studies. The extracted parameters included the patient's age, actual frame duration, count rate, total counts accumulated, largest image pixel value, scan velocity, and scan length. These variables are recognized to influence the technical quality of nuclear medicine images and may underlie some of the observed variance in image quality.

Metadata extraction was performed using the pydicom Python library. All identifying information was removed to preserve patient confidentiality, adhering to ethical data handling standards.

Descriptive statistics were computed for each metadata variable, and their distributions were analyzed. To explore associations between metadata and image quality clusters, Pearson's correlation coefficients were calculated using the scipy.stats module in Python, with significance set at $p < 0.05$.

3. RESULTS

Dimensionality reduction using Principal Component Analysis (PCA) was evaluated at varying levels - top 2, 3, and 32 components to analyze its impact on unsupervised clustering and classification based on ground truth formulated by nuclear medicine physicians. Clustering performance, assessed using Silhouette Score and Davies-Bouldin Index, was highest for the top 2 PCs (Silhouette: 0.4145; DB Index: 0.9151), indicating superior intra-cluster cohesion and inter-cluster separation. However, classification outcomes for this configuration were suboptimal, yielding the lowest accuracy (0.56), sensitivity (0.6083), and specificity (0.7789). In contrast, models using the top 3 and top 32 PCs achieved significantly higher classification accuracy (0.93), sensitivity (0.9312), and specificity (0.9648), despite demonstrating reduced clustering quality (Silhouette: 0.3010 and 0.1316; DB Index: 1.2198 and 2.2090, respectively). Among these, the 3-PC configuration offered a favorable trade-off, retaining substantial classification performance while maintaining moderately strong clustering metrics. Hence, based on a balanced consideration of both clustering coherence and classification effectiveness, the model employing the top 3 principal components was selected as the optimal dimensionality setting for this study.

A. PCA Explained Variance

Principal Component Analysis (PCA) was performed on the normalized and vectorized bone scan images to reduce dimensionality while preserving essential variance. The scree plot (Fig. 1(a)) demonstrated a steep decline in eigenvalues, indicating that the most informative features were concentrated in the initial components. Specifically, the first two principal components retained approximately 45% of the total variance, while the first three components captured about 55%. A cumulative variance of over 95% was achieved with the first 32 components(Fig. 1(b)).

B. Clustering Performance

K-means clustering (k = 3) applied to the PCA- transformed dataset yielded distinct groupings. Analysis of the cluster centroids revealed clear differences in pixel intensity patterns, spatial texture, and noise levels. Cluster 0 images exhibited lower contrast or higher noise; Cluster 1 images displayed moderate quality with noticeable but non-severe degradations; and Cluster 2 images were high-quality, showing crisp tracer uptake and uniform background.

C. Clinical Validation

To assess the clinical validity of the clusters, a subset of 100 images from 50 randomly selected studies was reviewed by a senior nuclear medicine physician. The number of images assigned to Cluster 0, Cluster 1, and Cluster 2 were 26, 40, and 34 respectively. Based on expert labels, the unsupervised model correctly categorized 93 out of 100 images, achieving a classification accuracy of 93%. This high concordance with clinical judgment affirms the utility of the clustering approach in approximating human quality assessment.

Figure 2 displays a t-distributed stochastic neighbour embedding (t-SNE) visualization of the three clusters; Figure 3 presents five random sample images from each cluster to provide a visual representation of the model's classification. Cluster 0 is associated with poor-quality images (Fig. 3(a)), while Cluster 1 encompasses images of moderate to good quality (Fig. 3(b)). Cluster 2, on the other hand, consists of high-resolution images with superior diagnostic clarity, representing excellent-quality images (Fig. 3(c)).

D. DICOM Metadata Extraction and Analysis

Acquisition parameters were extracted from the DICOM headers of all 203 bone scan studies. Key metadata included patient age, actual frame duration, count rate, total counts accumulated, largest image pixel value, scan velocity, and scan length. All images were acquired using a Low Energy High Resolution (LEHR) collimator, with an energy window setting of 140 ± 20%.

Table 1 presents descriptive statistics for key parameters from the 203 bone scan studies. The Actual Frame Duration averaged 120,330.05 seconds, while the Count Rate and Counts Accumulated showed substantial variation, with means of 3,978.14 and 2,202,242.51, respectively. The Largest Image Pixel Value ranged from 51 to 3,350. Patient Age had a mean of 36.10 years (range: 0–89), where a value of zero indicates patients under one year. For the 88 scans with complete spatial data, the Scan Velocity averaged 3.30 cm/min, and Scan Length had a mean of 1,757.66 cm.

Descriptive statistics grouped by image quality clusters (Table 2) reveal noticeable differences in acquisition parameters. Cluster 2, associated with higher-quality images, exhibited substantially greater mean and maximum values for both count rate and counts accumulated, alongside higher standard deviations. For instance, the maximum count rate in Cluster 2 reached 27,371 compared to 13,209 in Clusters 0 and 1, while the accumulated counts peaked at over 12 million versus approximately 7 million in the other clusters. This pattern suggests that higher image quality may be linked to more intense or prolonged acquisitions, potentially reflecting tailored imaging protocols or scanner configurations aimed at enhancing diagnostic clarity.

However, when formally assessed using Pearson's correlation coefficients, the relationships between image quality and both count rate ($r = 0.045$, $p = 0.362$) and counts accumulated ($r = 0.053$, $p = 0.291$) were found to be weak and statistically non-significant. These findings indicate that, despite the trends observed in the descriptive analysis, there is no strong or consistent linear association between acquisition parameters and perceived image quality across the dataset.

While metadata were not included in the clustering model, their analysis provides actionable insights for quality improvement in clinical imaging workflows.

4. DISCUSSION

This study introduces a novel, unsupervised framework for assessing image quality in nuclear medicine using whole-body bone scintigraphy scans. By integrating principal component analysis (PCA) with k-means clustering, the proposed method avoids reliance on ground-truth labels and enables objective, scalable quality categorization. Unlike traditional supervised deep learning approaches, which require large, annotated datasets and are often task-specific, our method is lightweight, interpretable, and broadly applicable across heterogeneous imaging protocols.

The clustering results demonstrated that PCA captured clinically relevant variations in image texture, contrast and tracer distribution, while k-means effectively partitioned the latent space into three distinct quality categories: poor, good, and excellent. The use of silhouette analysis and t-SNE visualization explained the internal validity and separability of the clusters.

Principal Component Analysis (PCA) followed by k- means clustering was applied to 406 bone scan images to evaluate the effect of dimensionality reduction on classification performance. Using only the top 2 principal components (PCs) resulted in poor accuracy (56%), while adding a third component significantly improved accuracy to 93%, which remained stable even with 32 PCs. This suggests that the third PC captures critical discriminative features not present in the first two, which may primarily reflect global intensity or shape rather than clinically relevant variations. Clustering quality metrics supported this trend, with the highest Silhouette Score observed for 2 PCs but optimal classification performance achieved with 3 PCs. Retaining more than 3 PCs did not yield further gains, indicating diminishing returns and potential redundancy. Therefore, the 3-PC configuration offered the best trade-off between preserving essential diagnostic information and avoiding unnecessary complexity, underscoring the importance of balanced dimensionality selection in medical image analysis.

In the classification of 100 sample bone scan images into three quality categories (poor, good, and excellent), the clustering model misclassified seven cases, some of which are displayed in Figure 4. These errors mostly involved assigning poor images to the good category, good to either poor or excellent, and excellent to good. While the overall accuracy remains high, these misclassifications highlight key limitations of the current model and the nature of the data. Such errors likely arise from the inherent subjectivity and gradual transitions in image quality, which do not always fit neatly into fixed categories [8]. PCA, though effective in reducing dimensionality, may exclude subtle yet clinically important features such as mild variations in noise or tracer distribution that are essential for accurate classification [9]. K-means clustering adds to this challenge by forming clusters based on visual similarity, without considering clinical meaning or context [10],[11]. Furthermore, expert disagreement in borderline cases may affect label consistency, making some misclassifications less about model error and more about ambiguous ground truth [12]–[17]. These findings highlight the importance of improving unsupervised methods by incorporating clinical context, metadata, or semi-supervised learning to improve classification performance in real-world applications.

While prior studies have successfully employed PCA and K-means clustering in medical imaging tasks such as tumor detection, general image segmentation, orthopedic analysis, and cancer diagnosis using modalities such as SPECT, PET/CT, and histological imaging [18]–[20], there remains a notable gap in their application for objective bone scan image quality assessment. Specifically, the literature does not address the classification of bone scans into discrete

quality categories like poor, good, and excellent using this approach. Our study uniquely bridges this gap by employing PCA for dimensionality reduction followed by K-means clustering to classify bone scan images based on quality. By systematically evaluating the effect of using 2, 3, and 32 principal components (PCs), we identified 3 PCs as optimal, achieving a classification accuracy of 93% and a specificity of 96%. These results not only validate the effectiveness of the PCA-K-means framework but also introduce a novel, unsupervised method for quantitative image quality classification in nuclear medicine imaging, offering a valuable tool for clinical decision support and quality assurance.

Key Advantages of the Proposed Framework

A major strength of the proposed framework lies in its ability to operate without ground-truth labels, making it inherently scalable and adaptable to large, unlabeled datasets across diverse clinical environments. This unsupervised approach eliminates the need for manual annotation, which is often time-consuming, expensive, and prone to subjective interpretation. By providing objective and repeatable classifications, the method reduces inter-observer variability and enhances consistency in quality assessment. Furthermore, its lightweight computational demands and reliance on interpretable techniques such as PCA make it suitable for real-time or near-real-time deployment within existing clinical workflows. These characteristics collectively position the model as a practical and robust solution for intelligent quality assurance in nuclear medicine imaging.

DICOM Metadata Insights

Incorporating DICOM metadata provided valuable context for interpreting cluster assignments. While analysis of acquisition parameters revealed moderate trends between image quality and factors such as count rate and total counts accumulated, formal evaluation using Pearson's correlation coefficients showed weak and statistically non-significant relationships. This suggests that image quality is likely influenced by multiple, possibly non-linear factors. Although DICOM metadata were not directly used in the clustering model, their alignment with cluster assignments supports their utility in future models for root-cause analysis or automated quality assurance.

Scan velocity values obtained from metadata were either missing or reported consistently as 3.33 or 3.00 cm/min. Although prior studies have demonstrated the impact of scan velocity on image quality and downstream analysis [21], its effect in this study is likely minimal due to the limited variability observed.

Overall, the metadata analysis underscores the potential for hybrid quality assessment models that combine image-based features with acquisition parameters. For instance, shorter scan durations may contribute to increased noise, while nonstandard zoom factors could influence spatial resolution.

Limitations and Future Work

This study has certain limitations. Firstly, it was based on a relatively smaller dataset, which may limit the generalizability of the findings. A larger dataset would likely improve the reliability and accuracy of the classification model, enhancing its robustness and applicability across diverse populations. Along with this, external validation across multiple institutions is needed to generalize the findings.

Future work will focus on expanding the dataset to enhance the generalizability and performance of the classification model in real-world settings. Additionally, we plan to explore hybrid models that integrate both image-based features and acquisition metadata. This approach could further improve classification accuracy, providing a more comprehensive framework for image quality assessment while also offering valuable insights for automated quality assurance systems.

5. CONCLUSION

We presented an unsupervised and interpretable IQA framework for 99mTc-MDP bone scintigraphy using PCA and K-means clustering. The method effectively classified images into three quality categories - 'Poor', 'Good' and 'Excellent' without the need for annotated datasets. It achieved 93% accuracy, 93.12% sensitivity, and 96.48% specificity.

6. DISCLOSURE

No potential conflicts of interest relevant to this article exist.

REFERENCES

1. Z. Wang, A. C. Bovik, H. R. Sheikh, and E. P. Simoncelli, “Image quality assessment: From error visibility to structural similarity,” IEEE Transactions on Image Processing, vol. 13, no. 4, pp. 600– 612, Apr. 2004.
2. International Atomic Energy Agency, SPECT/CT Atlas of Quality Control and Image Artefacts, Vienna, Austria: IAEA, 2019.
3. H. M. S. S. Herath, H. M. K. K. M. B. Herath, N. Madusanka, and B.-I. Lee, “A systematic review of medical image quality assessment,” J. Imaging, vol. 11, p. 100, Apr. 2025.
4. A. K. Pandey, A. Sharma, P. D. Sharma, C. S. Bal, and R. Kumar, “Automated detection of poor-quality scintigraphic images using machine learning,” World J. Nucl. Med., vol. 21, pp. 276–282, 2022.
5. H. R. Sheikh and A. C. Bovik, “Image information and visual quality,” IEEE Transactions on Image Processing, vol. 15, no. 2, pp. 430–444, Feb. 2006.
6. I. T. Jolliffe, “Principal component analysis,” in Springer Series in Statistics, 2nd ed. New York: Springer, 2002.
7. M. Halkidi, Y. Batistakis, and M. Vazirgiannis, “On clustering validation techniques,” Journal of Intelligent Information Systems, vol. 17, no. 2, pp. 107–145, 2001.
8. L. Shen, M. Margolies, J. Rothstein, E. Fluder, R. McBride, and W. Sieh, “Deep learning to improve breast cancer detection on screening mammography,” Sci. Rep., vol. 9, no. 1, pp. 1–12, 2019.
9. A. L. Beam and I. S. Kohane, “Big data and machine learning in health care,” JAMA, vol. 319, no. 13, pp. 1317–1318, Mar. 2018.
10. A. K. Jain, M. N. Murty, and P. J. Flynn, “Data clustering: A review,” ACM Computing Surveys, vol. 31, no. 3, pp. 264–323, Sep. 1999.
11. S. Lloyd, “Least squares quantization in PCM,” IEEE Transactions on Information Theory, vol. 28, no. 2, pp. 129–137, Mar. 1982.
12. Z. Huemann, C. Lee, J. Hu, S. Y. Cho, and T. J. Bradshaw, “Domain-adapted large language models for classifying nuclear medicine reports,” Radiology: Artificial Intelligence, vol. 5, no. 6, p. e220281, Nov. 2023.
13. G. Geethakumari, et al., “Machine learning-based assignment of Deauville scores is comparable to interobserver variability on interim FDG PET/CT images of pediatric Hodgkin lymphoma,” Journal of Nuclear Medicine, vol. 61, suppl. 1, p. 1434, Jan. 2020.
14. T. Georgi, et al., “Interobserver variability in interim PET assessment in Hodgkin lymphoma: causes and suggestions for improvement,” PLoS One, vol. 18, no. 3, e0283694, Mar. 2023.
15. N. G. Mikhaeel, et al., “Interobserver agreement on automated metabolic tumor volume measurements in interim PET scans of lymphoma patients,” Journal of Nuclear Medicine, vol. 62, no. 11, pp. 1531–1537, Nov. 2021.
16. S. F. Barrington, et al., “Validation of Deauville Score for Response Evaluation in Hodgkin's Lymphoma,” Diagnostics (Basel), vol. 13, no. 1, p. 157, Jan. 2023.
17. A. Gallamini, et al., “The Deauville criteria for interim PET in lymphoma: interobserver agreement and clinical implications,” European Journal of Nuclear Medicine and Molecular Imaging, vol. 42, no. 10, pp. 1502–1510, Oct. 2015.
18. F. Cabitza, A. Locoro, and G. Banfi, “Machine learning in orthopedics: a literature review,” Frontiers in Bioengineering and Biotechnology, vol. 6, p. 75, Jul. 2018.
19. B. M. Rashed and N. Popescu, "Critical analysis of the current medical image-based processing techniques for automatic disease evaluation: Systematic literature review," Sensors, vol. 22, no. 18, p. 7065, 2022.
20. Z. Chen, X. Chen, and R. Wang, "Application of SPECT and PET/CT with computer-aided diagnosis in bone metastasis of prostate cancer: a review," Cancer Imaging, vol. 22, no. 1, p. 18, Apr. 2022.
21. A. Anand, M. J. Morris, R. Kaboteh, M. Reza, E. Trägårdh, N. Matsunaga, L. Edenbrandt, A. Bjartell, S. M. Larson, and D. Minarik, “A preanalytic validation study of automated bone scan index: Effect on accuracy and reproducibility due to the procedural variabilities in bone scan image acquisition,” Journal of Nuclear Medicine, vol. 57, no. 12, pp. 1865–1871, Dec. 2016.

TABLES

Table 1 : Descriptive Statistics of Important Attributes of the Data

***Abbreviations: A**, Actual Frame Duration(in seconds); **B**, Count Rate; **C**, Counts Accumulated; **D**, Largest Image Pixel Value; **E**, Patient Age(in years); **F**, Scan Velocity(in cm/min); **G**, Scan Length(in cm). *A value of zero indicates that some patients were less than one year of age.*

	A	B	C	D	E	F	G
count	203	203	203	203	203	88	88
mean	120330.05	3978.14	2202242.51	260.39	36.10	3.30	1757.66
std	7311.62	2313.14	1095480.75	372.74	21.42	0.19	185.43
min	90000	1138	542350	51	0 *	2.67	919
25%	120000	2789.5	1580103	111.5	18.5	3.33	1699.75
50%	120000	3569	2011212	158	36	3.33	1781.5
75%	120000	4447.5	2563464	236.5	54	3.33	1859
max	160000	27371	12440319	3350	89	4.43	1997

Table 2 : Summary Statistics of Count Rate and Accumulated Counts by Image Quality Cluster

	Count Rate	Counts Accumulated				
Cluster	std	min	max	std	min	max
0	1702.039609	1742	13209	8.256157e+05	923944	7192678
1	1818.718158	1138	13209	9.057488e+05	542350	7192678
2	3285.660801	2072	27371	1.508013e+06	1065558	12440319

FIGURE LEGENDS

Figure 1 Legend : Scree Plots illustrating **(a)** the explained variance versus the number of principal components, and **(b)** the cumulative explained variance versus the number of principal components.

Figure 2 Legend : t-SNE visualization of clustered bone scan images in reduced PCA space (k = 3). The three clusters show clear separation, corresponding to poor, moderate, and high-quality image categories identified by the model.

Figure 3 Legend : Five random sample images (both anterior and posterior) from **(a)** Cluster 0 (poor-quality bone scans). **(b)** Cluster 1 (good-quality bone scans). **(c)** Cluster 2 (excellent-quality bone scans).

Figure 4 Legend : Representative examples of misclassified bone scan images.

(a) Ground truth: good quality (class 1); predicted: excellent quality (class 2). **(b)** Ground truth: excellent quality (class 2); predicted: good quality (class 1). **(c)** Ground truth: good quality (class 1); predicted: poor quality (class 0). **(d)** Ground truth: poor quality (class 0); predicted: good quality (class 1).

FIGURES

Figure 1 :

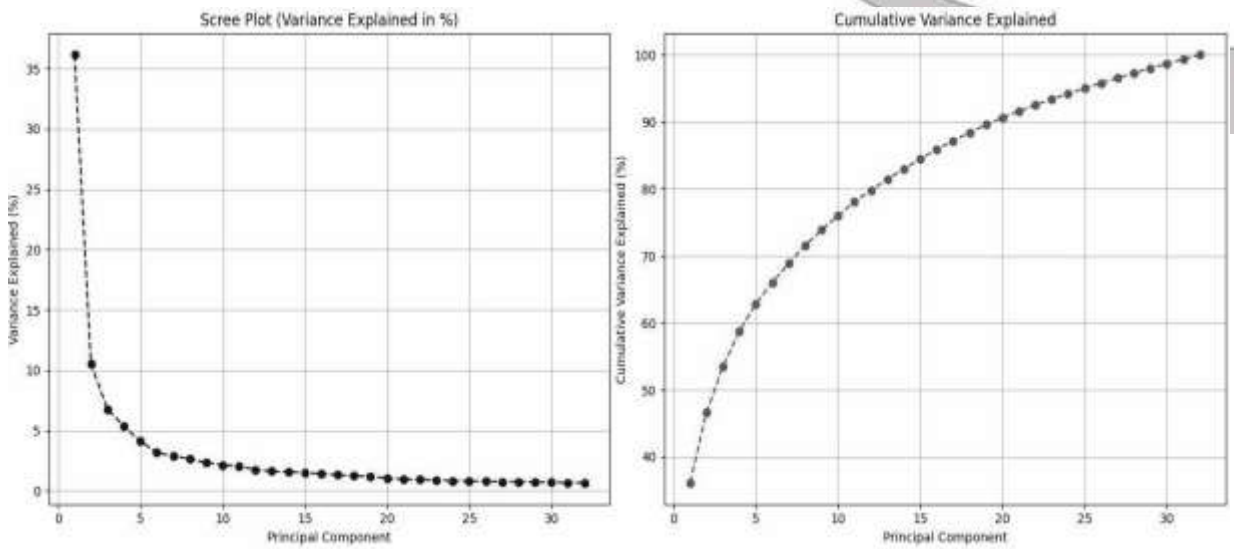
Scree Plot (Variance Explained in %)
Variance Explained (%)
Principal Component
Cumulative Variance Explained
Cumulative Variance Explained (%)
Principal Component

Figure 2 :

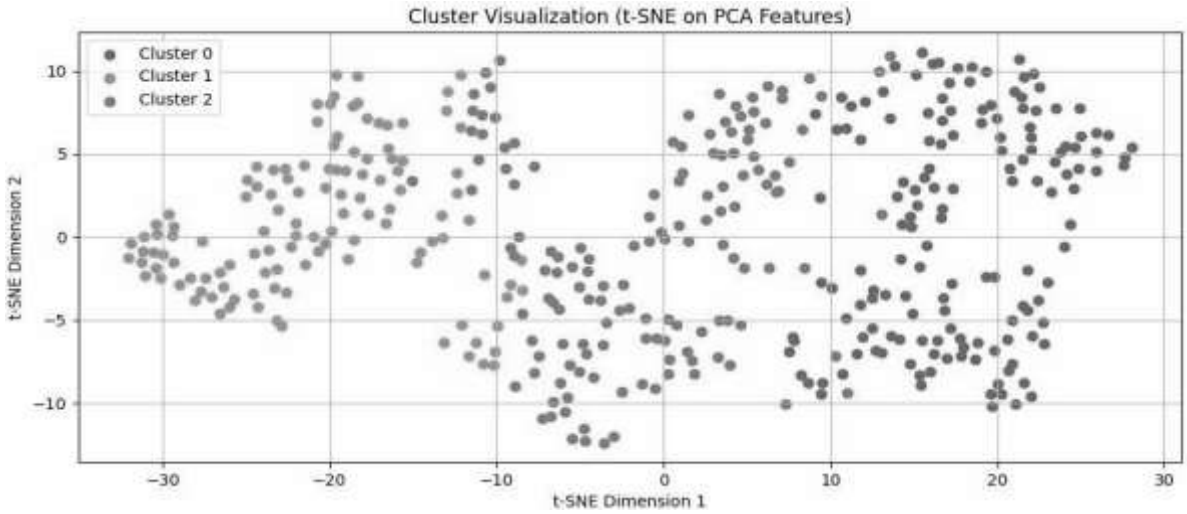
Cluster Visualization (t-SNE on PCA Features)
Cluster 0
Cluster 1
Cluster 2
t-SNE Dimension 2
t-SNE Dimension 1

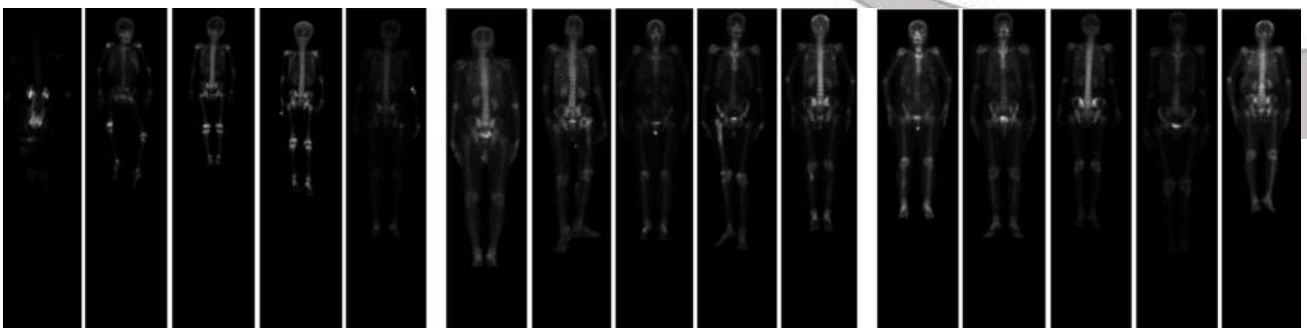

Figure 3 : (a,b,c from left to right)

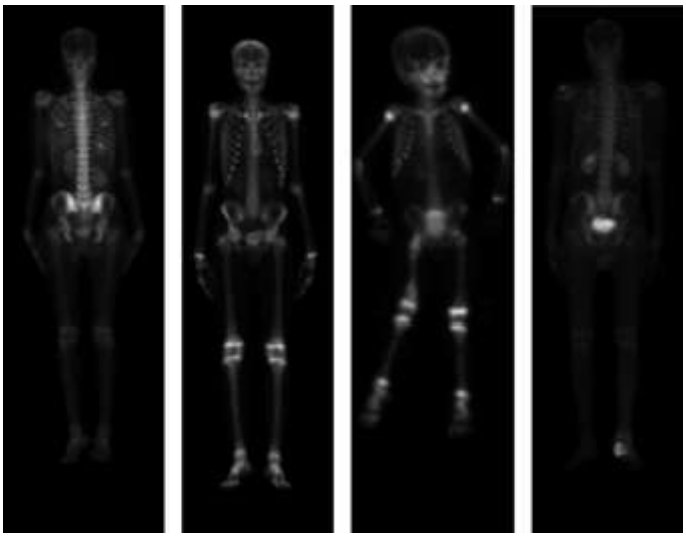

Figure 4 : (a,b,c,d from left to right)